

## ENGINEERING

# Untethered small-scale magnetic soft robot with programmable magnetization and integrated multifunctional modules

**Yue Dong<sup>1</sup>, Lu Wang<sup>1</sup>, Neng Xia<sup>1</sup>, Zhengxin Yang<sup>1</sup>, Chong Zhang<sup>1</sup>, Chengfeng Pan<sup>1</sup>, Dongdong Jin<sup>1</sup>, Jiachen Zhang<sup>2</sup>, Carmel Majidi<sup>3\*</sup>, Li Zhang<sup>1,4,5\*</sup>**

Intelligent magnetic soft robots capable of programmable structural changes and multifunctionality modalities depend on material architectures and methods for controlling magnetization profiles. While some efforts have been made, there are still key challenges in achieving programmable magnetization profile and creating heterogeneous architectures. Here, we directly embed programmed magnetization patterns (magnetization modules) into the adhesive sticker layers to construct soft robots with programmable magnetization profiles and geometries and then integrate spatially distributed functional modules. Functional modules including temperature and ultraviolet light sensing particles, pH sensing sheets, oil sensing foams, positioning electronic component, circuit foils, and therapy patch films are integrated into soft robots. These test beds are used to explore multimodal robot locomotion and various applications related to environmental sensing and detection, circuit repairing, and gastric ulcer coating, respectively. This proposed approach to engineering modular soft material systems has the potential to expand the functionality, versatility, and adaptability of soft robots.

Copyright © 2022  
The Authors, some  
rights reserved;  
exclusive licensee  
American Association  
for the Advancement  
of Science. No claim to  
original U.S. Government  
Works. Distributed  
under a Creative  
Commons Attribution  
NonCommercial  
License 4.0 (CC BY-NC).

## INTRODUCTION

There has been tremendous progress in recent years in the development of small-scale, untethered soft robotic systems that are capable of programmable shape morphing through magnetic fields, light, temperature, chemical cues, and other forms of external or environmental stimulation. Such systems have enabled an increasing number of promising applications in cargo grasping (1–7), intelligent electronics (8–12), precision medicines (1, 8, 13–17), and bionics (18–23). However, further progress in creating stimuli-responsive soft robots that are capable of mimicking the rich multifunctionality, agility, and physical adaptability of living creatures (24) remains a notable challenge (25, 26). One main limitation is how to integrate multiple functional modules with dissimilar material compositions into one soft robot (27–31). While numerous examples of stimuli-responsive materials capable of reversible shape change, locomotion, and sensing have been developed, there are relatively few examples of heterogeneous architectures that combine these functionalities into a single integrated system. This is particularly true for magnetically activated soft robots, for which the magnetization profile can be precisely controlled to achieve programmable structural changes for multimodal motions and diverse applications (1, 8, 27). These existing robots lack the ability to close the loop between sensing, signal processing, and actuation (32). In this respect, simultaneous integration of programmable structural changes and various functional modules remains a key scientific challenge in the development of

magnetically responsive material systems that exhibit robot intelligence (24, 33).

Another limitation with existing magnetic soft robots is that current methods of manufacturing, material design, geometry change, and operation result in materials that form bending and folding deformations. Most of these methods involve the creation of discrete magnetization (uniform magnetization) profiles of hard magnetic particles [neodymium-iron-boron (NdFeB) and chromium dioxide] by altering the orientation of magnetized microparticles (13) and nanomagnets (20) locally or globally within the soft robot. This is accomplished using a variety of fabrication techniques, including three-dimensional (3D) printing (8, 34, 35), lithography (2), electron beam lithography of nanomagnets (20), laser heating (3, 9), spraying (13), and magnetized modules assembly with dynamic covalent bonds (36, 37) and bonding agent (14, 38). Although template-assisted magnetic programming allows continuous magnetization (nonuniform magnetization) for simple curved deformation (1, 39), transformative soft robots containing several curved structures are difficult to fabricate using this method due to the requirement of shape conformability, intricate template geometries, and demanding operations. Alternatively, magnetized modules assembly has the potential to achieve this goal, but only the concept for these modular architectures has been proposed (14). In addition, assembly of magnetized modules avoids the processing limitation of previous methods to create arbitrary 3D geometries (14). However, the laborious connecting steps between individual magnetized modules increase fabrication duration and complexity. Thus, a more efficient approach should be developed to achieve programmable uniform and nonuniform magnetization assembly and 2D and 3D geometries of soft robots.

With respect to multifunctional soft robots, a universal strategy is to integrate various functional modules [logical microfluidic systems (40), temperature sensing (27), light sensing (41), biosensing (42, 43), superhydrophobic surfaces (27), cell cages (14), etc.] with soft compliant materials. These modules are composed of micro/nanoparticles, circuit wiring, and microelectronic components. Considering the

<sup>1</sup>Department of Mechanical and Automation Engineering, The Chinese University of Hong Kong, Shatin, New Territories, Hong Kong SAR, China. <sup>2</sup>Department of Biomedical Engineering, City University of Hong Kong, Kowloon, Hong Kong SAR, China.

<sup>3</sup>Department of Mechanical Engineering, Carnegie Mellon University, Pittsburgh, PA 15213, USA. <sup>4</sup>Department of Surgery, The Chinese University of Hong Kong, Shatin, New Territories, Hong Kong SAR, China. <sup>5</sup>T Stone Robotics Institute, The Chinese University of Hong Kong, Shatin, New Territories, Hong Kong SAR, China.

\*Corresponding author. Email: lizhang@mae.cuhk.edu.hk (L.Z.); cmajidi@andrew.cmu.edu (C.M.)

soft and thin structure of magnetic soft robots, it is important that the introduction of functional modules does not hinder their natural mechanics and deformability. Meanwhile, a general material architecture should be developed to achieve seamless integration of various modules. Wu's group (27) achieved various functional particles infusion in different regions of soft robots for deformation, superhydrophobic surface, and sensing. Sitti's group (14) integrated microcages at the surface of soft robots for cell transport, which has no apparent influence on the deformation of soft robots. Although some advanced functions have been integrated, extra connecting steps are needed for functional modules integration, and delamination may occur because of different material properties and limited bonding agent choice. Therefore, the integration of various functional modules with different material properties and forms still requires further exploration to bring more intelligent magnetic soft robots. Furthermore, some functional modules need to be conveniently replaced once they are used or damaged for sustainable use of soft robots.

Here, we address these challenges with a modular soft magnetic architecture in which individual units contained NdFeB microparticles with prescribed magnetization profiles (uniform or non-uniform). The modular magnetization units are directly embedded into the network of adhesive sticker layers to form magnetic soft robots with arbitrary 2D and 3D geometries. Multiple functional modules with different material properties and formation factors (e.g., particles, papers, films, foams, and electronic components) can be seamlessly integrated through robust adhesion to form connected networks. The recyclable adhesive sticker allows some functional modules to be easily replaced after use. As proof-of-concept demonstrations of multifunctional soft robots, we introduce temperature and ultraviolet (UV) light sensors, pH detectors, polydimethylsiloxane (PDMS) foams, radio frequency identifier (RFID), and drug loading films and demonstrate the ability to create magnetic soft robots capable of multimodal motions and applications in environmental sensing and detection, positioning, circuit repairing, and gastric ulcer therapy. Our approach simplifies the fabrication steps for intelligent soft robots with customized shape deformation and function, enabling the possibilities of their applications in multiple fields.

## RESULTS

### Design and fabrication of programmable and multifunctional magnetic soft robots

The schematic diagram of fabrication and application for multifunctional soft robots is illustrated in Fig. 1. In the fabrication process, patterns composed of NdFeB microparticles are first magnetized by template-assisted method (fig. S1) with a magnetizer (39). NdFeB patterns with either uniform (in-plane and out-of-plane) or non-uniform magnetization profiles are achieved in this manner. Next, magnetized NdFeB patterns are selectively embedded into the adhesive sticker network of the top and bottom sides of the double-sided adhesive to form the programmable magnetic body of the soft robotic system. The position and direction of magnetized patterns are determined by the desired shapes and structural changes of soft robots. In this process, no additional connecting step is required due to the overall network and tackiness of double-sided adhesive layers. Then, the magnetic soft robots are cut out from the double-sided adhesive, after which they are powered by a spatially non-uniform magnetic field. Within the actuating magnetic field, the 3D deformation of a soft robot is primarily driven by magnetic torques

that align the local magnetization with the field direction, and then the magnetic forces increase or decrease the robot's deformation depending on the relationship between the reoriented magnetization of the initially torque-driven deformation with the direction of magnetic field gradient (44, 45). The magnetic response of the robot will either involve folding or continuous structural changes depending on whether it is programmed with uniform or nonuniform magnetization profiles, respectively. We note that the regions on both sides of the double-sided tape that do not contain NdFeB microparticles can be populated with microelectronics, circuit wiring, and other elements to support additional robotic functionalities. Next, functional modules are seamlessly incorporated into the inner network (temperature and UV light sensing particles) or outer surface (pH paper, PDMS foam, and RFID) by adhesion to these nonmagnetized regions. As a mature commercial product, adhesive sticker has been developed and refined to tightly bond various materials under light pressure, which is beneficial for robust interfacing of modular units. The resulting soft robots can perform multimodal motion and achieve environmental sensing, positioning, and circuit repair by combining the specialized functions of each unit.

### The programming and transfer of magnetized NdFeB patterns

The synthesis and transfer of prescribed NdFeB patterns and magnetization profiles (either uniform or nonuniform) are the basis of the magnetic soft robots. Figure 2A describes these processes in detail. First, a patterned wax mask (10.4 μm in thickness) is printed onto the polyetherimide (PEI) tape with a thin adhesive layer by a wax printer (Fig. 2B). The PEI tape loses its stickiness in the regions coated with wax. NdFeB microparticles are then adhered onto the exposed regions of the PEI tape, thereby forming the NdFeB patterns (Fig. 2C, fig. S2A, and movie S1). Next, the PEI tape is soaked in ethyl acetate solution for 5 min to remove the wax mask. Because of the swelling of the adhesive layer, the wax pattern on the surface of PEI tape can be easily removed after soaking and slightly shaking (fig. S2B and movie S1). However, the NdFeB patterns (Fig. 2D) are stably fixed into the network of adhesive layer, and nearly no NdFeB microparticles are observed after attracting ethyl acetate solution with a magnet (fig. S2C). The patterned NdFeB on PEI tape is henceforth referred to as a NdFeB/PEI film. From its cross-sectional scanning electron microscopy (SEM) images (Fig. 2F), we find that a small part of NdFeB microparticles volume is embedded within the thin adhesive layer, indicating the excellent stickiness of the adhesive layer. The planar resolution of the patterned NdFeB features can reach 40 μm (fig. S3), which lays the foundation for small-scale magnetic soft robots.

We also investigate the ability to transfer the patterned NdFeB layer from PEI tape to a double-sided tape. The NdFeB/PEI film is placed onto the double-sided tape with the NdFeB side facing down. After applying pressure, a large portion of the NdFeB microparticles is transferred to the thick adhesive layer of the double-sided tape (Fig. 2E). Upon peeling off the PEI tape, most of the NdFeB particles are transferred into the double-sided tape (Fig. 2G and movie S1). However, some NdFeB microparticles still remain in the PEI tape, which is ascribed to its nonuniform size as displayed in SEM images (fig. S4). Moreover, some small NdFeB microparticles are deeply embedded into the adhesive layer of the PEI tape or do not make initial contact with the double-sided tape due to interference from larger NdFeB microparticles during the transfer process (fig. S5). However, although larger NdFeB microparticles can prevent some

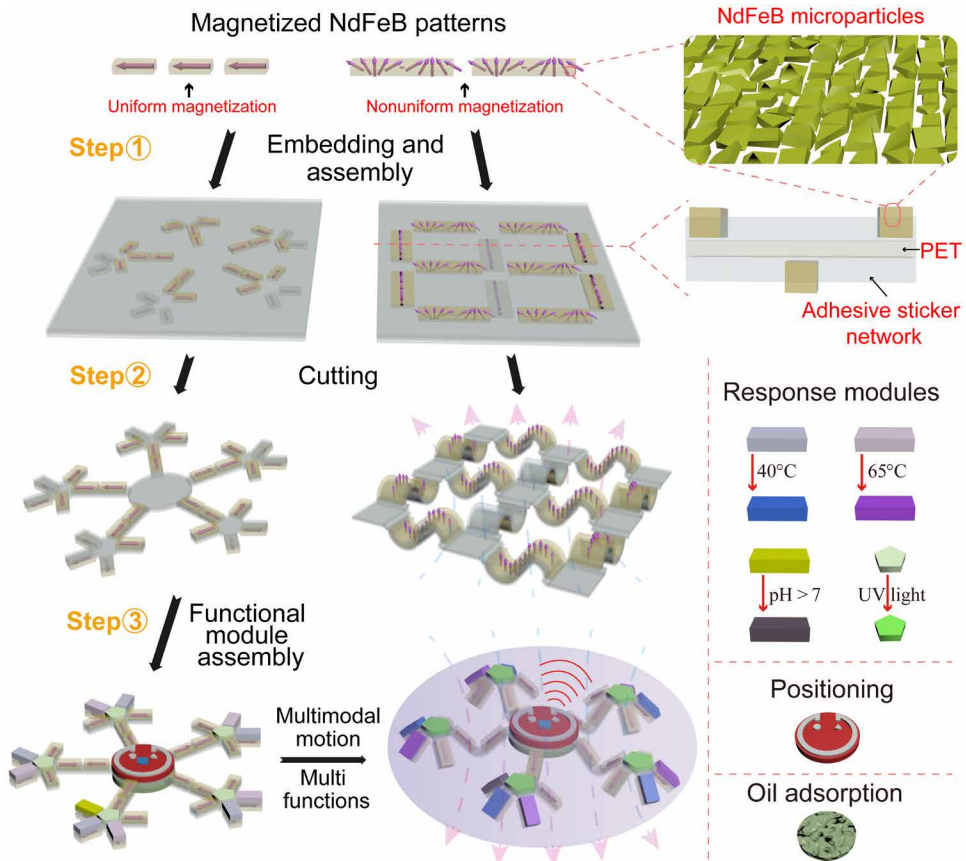


**Fig. 1. The schematic diagram of integrating magnetized NdFeB patterns and functional modules for programmable and multifunctional magnetic soft robots and their applications.** PET, polyethylene glycol terephthalate.

of the smaller particles from transferring, they are nonetheless important since they provide the soft robot with a stronger magnetic force response (fig. S6). Meanwhile, a thicker adhesive layer is needed to accommodate larger NdFeB microparticles. As shown in Fig. 2H and figs. S7 and S8, we investigate the transfer of unmagnetized and magnetized NdFeB microparticles with average sizes of 38.0, 75.0, and 150.0  $\mu\text{m}$  on double-sided tapes with different thicknesses (0.3, 0.5, and 1.0 mm). These NdFeB microparticles are uniformly distributed into the double-sided tapes, as also demonstrated by the SEM image (Fig. 2I). No agglomeration happens for magnetized NdFeB microparticles, demonstrating that NdFeB microparticles are stably and separately fixed into the adhesive layer, which is essential for uniform and consistent deformation of soft robots. Therefore, our proposed strategy is suitable for fabricating magnetic soft robots with different thicknesses. As the thickness of double-sided tapes increases, more NdFeB microparticles are inserted into the adhesive layer, and the transfer efficiency increases. As the size of NdFeB microparticles increases, their transfer efficiency in double-sided tapes with the same thickness decreases. We calculate their transfer efficiency by measuring the weight of NdFeB microparticles in the PEI tape before and after the transfer (Fig. 2K). All measured transfer efficiencies are beyond 85.0%, ensuring that our strategy can be efficiently used to assemble NdFeB patterns for magnetic soft robots.

We also compare the magnetization profiles of magnetized NdFeB patterns before transfer (in PEI) and after transfer (in double-sided

tapes) captured by a magneto-optical microscope (Fig. 2J). The NdFeB/PEI films are magnetized by the template-assisted method (fig. S1) (39). We find that the magnetization profiles remain the same, with no obvious difference observed for uniform (in-plane and out-of-plane magnetization) or nonuniform magnetization. This observation indicates that NdFeB microparticles do not rotate and displace easily in the process of pressing and scratching due to the strong cohesion and elasticity of the adhesive sticker, which is critical for the successful fabrication of the anticipated magnetic soft robots with high fidelity in magnetization profiles. The NdFeB microparticles are also stably fixed into the double-sided tape and cannot be rotated or moved even after repeated stimulation with magnetic field (100 mT) for 2000 cycles (Fig. 2, L and M). Two rectangular NdFeB patterns with uniform and nonuniform magnetization are inserted into the double-sided tape (10 mm by 2 mm by 0.03 mm and 10 mm by 2 mm by 0.1 mm) to demonstrate their stability. Unexpectedly, nearly no height and curvature changes are observed, indicating that soft robots fabricated by our strategy can be used for a long time even when using the largest NdFeB microparticles (150.0  $\mu\text{m}$ ) and thinnest double-sided tape (0.03 mm). In addition, the soft robots are also stable after ultrasonic in water for 1 hour and magnetic stimulation in HCl solution, NaOH solution, ethanol, gastric fluids, blood, saliva, and urine for 2 hours (fig. S9). Therefore, the proposed strategy for fabrication and transfer of magnetized NdFeB patterns is simple, robust, and suitable for developing programmable magnetic soft robots.

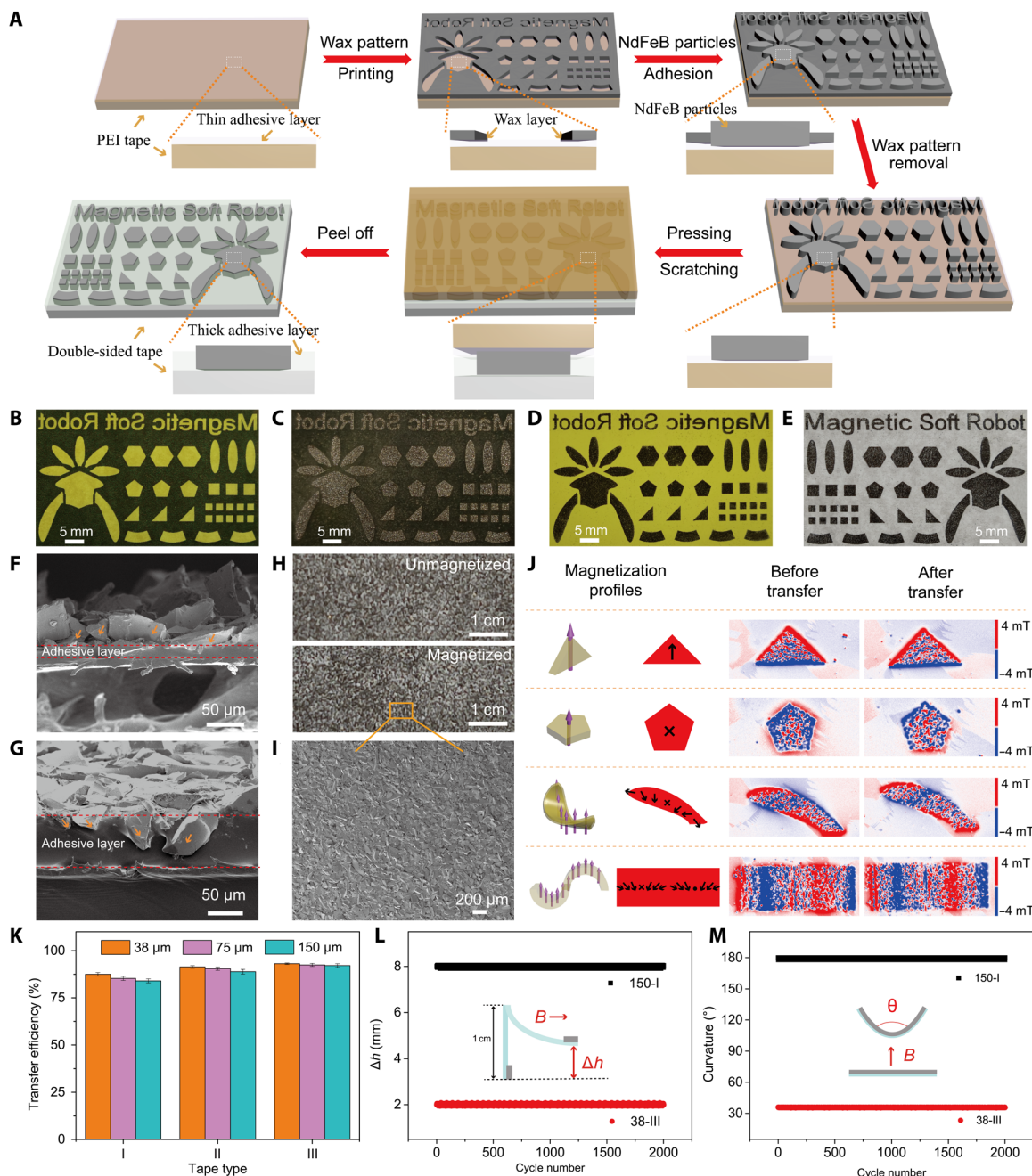


**Fig. 2. The fabrication and transfer of NdFeB patterns.** (A) The fabrication process of NdFeB patterns. The optical images of (B) wax mask on PEI tape, (C) NdFeB patterns and wax mask on PEI tape, (D) NdFeB patterns on PEI tape after wax removal, (E) NdFeB patterns in the double-sided tape. The cross-sectional SEM images of NdFeB micro-particles on (F) PEI and (G) double-sided tapes. (H) The enlarged optical images and (I) SEM image of magnetized and unmagnetized NdFeB microparticles in double-sided tapes with different thicknesses. (J) The magneto-optical microscope images of magnetized NdFeB patterns [uniform (in-plane and out-of-plane) and nonuniform magnetization] before transfer and after transfer. (K) The transfer efficiency of NdFeB microparticles in double-sided tapes. The stability of NdFeB patterns with (L) uniform and (M) nonuniform magnetization in the double-sided tape after magnetic stimuli for 2000 times.

### The assembly process and structural changes of soft robots with 2D geometries

We further assemble several programmable magnetic soft robots with uniform and nonuniform magnetization and 2D and 3D geometries to explore their shape changes. The relationship between the shape of the template and the magnetization profiles of all NdFeB

patterns has been provided to understand the structural changes of the assembled soft robots (fig. S1). Their specific geometrical parameters are reported in fig. S10. The thinnest double-sided tape (0.03 mm) and medium-sized NdFeB microparticles (75.0  $\mu\text{m}$ ) are selected to ensure the dexterous shape changes and fast magnetic response of soft robots. Although larger NdFeB microparticles

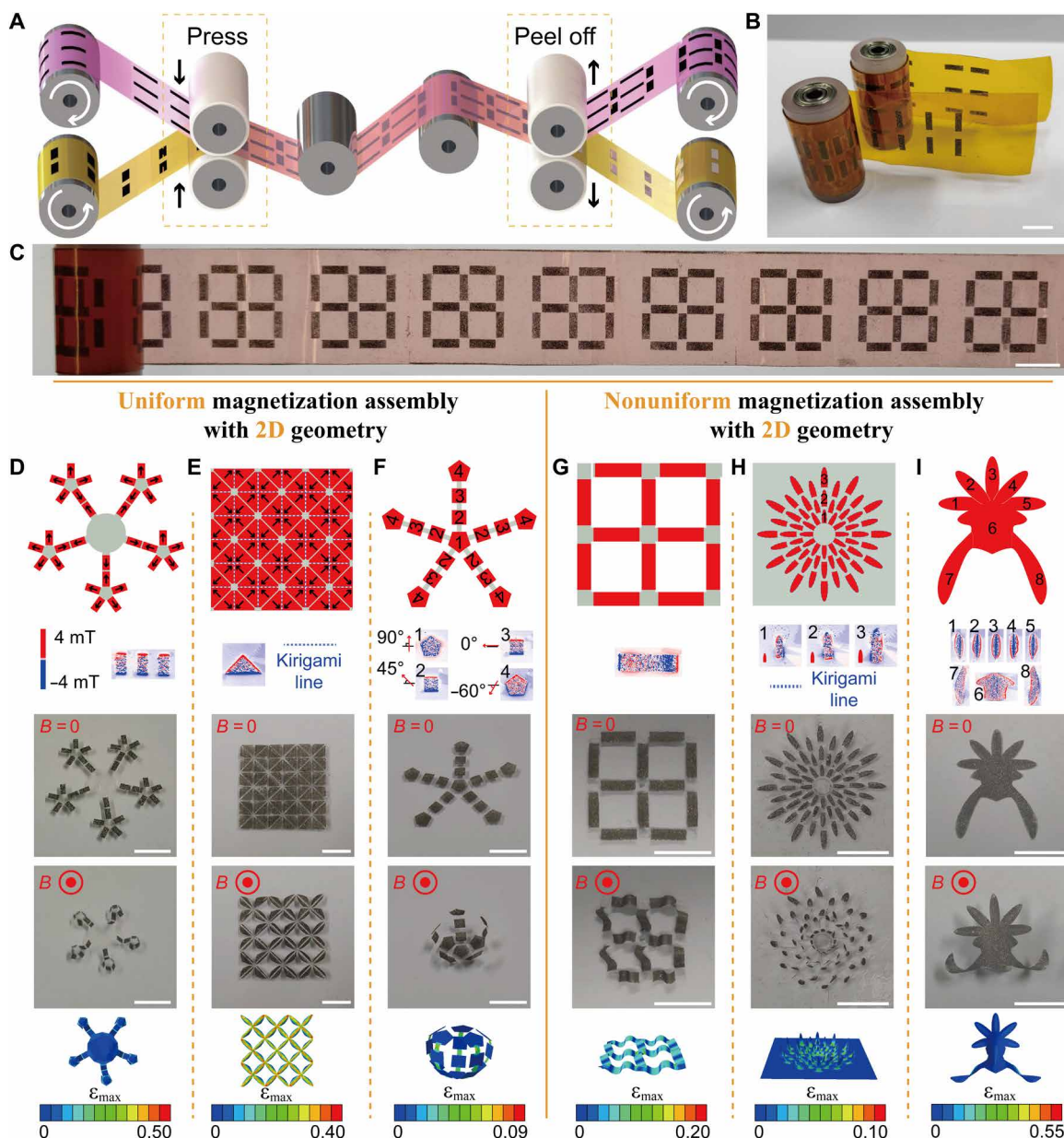


**Fig. 3. The soft robots with uniform and nonuniform magnetization assembly and 2D geometries.** (A) The schematic diagram of assembly process with roll-to-roll technology. (B) Magnetized NdFeB patterns fixed on the roller. (C) The assembled soft robots with high reproducibility. The designed shapes with distributed magnetizations, optical images before and after magnetic stimulus, and simulated deformation results of soft robots with 2D geometries fabricated by (D to F) uniform magnetization assembly and (G to I) nonuniform magnetization assembly. [The inset images are the magneto-optical microscope images of magnetized NdFeB patterns. Scale bars, 1.0 cm; color bars, the range of “maximum principal strain (logarithmic strain)”].

(150.0  $\mu\text{m}$ ) can provide faster magnetic response, too large of a structural change will affect the overall deformation of small-scale soft robots. As shown in Fig. 3A and movie S2, we transfer and assemble magnetized NdFeB patterns one by one into the double-side tape and demonstrate mass production of programmable magnetic soft robots using roll-to-roll manufacturing. The different magnetized NdFeB patterns are fixed onto different rollers according to the shape and magnetization profiles of soft robots. For example, magnetized rectangular NdFeB patterns with different directions are first uniformly distributed onto two PEI tapes in a complementary form (Fig. 3B). After transferring two consecutive times with the

custom-made roll-to-roll device, the spatially patterned magnetic soft robots can be reproduced in a high-throughput manner (Fig. 3C and movie S2). We believe that more advanced roll-to-roll device can be designed and optimized to produce complex programmable soft robots composed of dozens of NdFeB patterns with one process.

The assembly of NdFeB patterns can also be easily achieved manually (fig. S11 and movie S2). A soft robot with magnetization directions (black arrows) printed on an A4 paper is taped at the bottom of the double-sided tape (fig. S11). Next, the soft robots are acquired by cutting along their profiles. No connecting step is needed in all of these processes. Figure 3 (B to G) displays soft robots with 2D

geometries and their shape changes [optical images and simulation results [these simulations are conducted using a user-element subroutine (UEL) in ABAQUS (8, 46)]. Magnetic field generated by a magnet is used to induce the deformation of assembled soft robots (fig. S12). To suppress the influence of magnetic force, a large disc-shaped magnet with the diameter of 8 cm is applied to minimize the magnetic field gradient (47). Thirty identical rectangular NdFeB patterns with in-plane magnetization are assembled to form a multi-legged robot that is powered by an external magnetic field, which causes the legs to contract (Fig. 3B and movie S3). Similarly, 72 identical triangular NdFeB patterns with in-plane magnetization are assembled to enhance the deformation capability through using a kirigami design (Fig. 3C). NdFeB patterns are partially separated by cutting the tape along blue dotted lines. Upon stimulation by a magnetic field, all back-facing triangular NdFeB patterns approach each other to form complex 3D deformation (Fig. 3C and movie S3). As a typical deformation of out-of-plane magnetizations, the assembled soft robot fabricated by 16 NdFeB patterns with four out-of-plane magnetizations can transform into a polyhedron (Fig. 3D and movie S3). In addition to the uniform magnetization assembly above, nonuniform magnetization assembly has been easily achieved to create more complex deformation shapes with multiple curved structures. Twelve identical rectangular NdFeB patterns with S-shaped deformation are assembled to form a metamaterial structure that can expand and contract both in length and width simultaneously and has enabled multifunctional applications (Fig. 3E and movie S3). The structures of blooming chrysanthemum and *Dendrophylax lindenii* are also constructed (Fig. 3, F and G), which can be used to study and use plant behavior. Sixty petal-shaped NdFeB patterns of different sizes with arc-shaped deformation are assembled to mimic the structure of blooming chrysanthemum (Fig. 3F and movie S3). These petals can swing simultaneously and quickly with the movement of an external magnet, suggesting the potential to mimic the function of cilia for pumping and mixing biological fluids. The *D. lindenii* is assembled by six arc-shaped structures and two helical structures generated by eight simple NdFeB patterns (Fig. 3G and movie S3). These patterns are split from the planar structure of *D. lindenii*. All of the above examples demonstrate the versatility of our method to create soft robots with a wide range of uniform and nonuniform magnetization profiles and 2D geometries. The detailed assembly processes are presented in fig. S11. These simulation results in Fig. 3 (B to G) are reasonably close to the actual deformation of the soft robots. We attribute the small differences between simulation and experiment to the following three factors: (i) spatially non-uniform magnetic field in experiments, (ii) manual assembling process, and (iii) imperfect and discontinuous magnetization profiles in the simulated models (see more discussion in text S1).

### The assembly process and structural changes of soft robots with 3D geometries

Soft robots with 3D geometry can also be constructed by using the tackiness of the double-sided tape. The two ends of the planar structures are firmly taped together to form 3D structures, which cannot be torn apart even if they are loaded with objects thousands of times their weight (fig. S13). Two columnar structures are exhibited in Fig. 4 (A and C). The columnar structure with 24 square magnetized NdFeB patterns (uniform magnetizations) transforms into an epsilon-shaped structure upon stimulation by the magnetic field (Fig. 4A and movie S3). The columnar structure with six rectangular magnetized

NdFeB patterns (nonuniform magnetizations) and 12 square magnetized NdFeB patterns (uniform magnetizations) either contracts or expands along the radial direction under the stimulation of external magnetic field (Fig. 4C and movie S3). A similar structural change has been successfully applied in capsule and drug delivery (48, 49). Furthermore, more complex 3D soft robots are constructed by bonding simple 3D structures with self-adhesive. As exhibited in Fig. 4B, 16 square magnetized NdFeB patterns (uniform magnetizations) are first distributed in the rectangular stripes of the double-sided tape. Next, two ends of rectangular stripes are bonded together to form simple dumbbell structures. Three of these dumbbell structures are then bonded together in a side-by-side manner to form a 3D soft robot. After stimulation with an external magnetic field, the robot folds and undergoes shape change into another 3D structure. Likewise, four rectangular NdFeB patterns with uniform and non-uniform magnetizations are first assembled, folded, and bonded to form the simple triangular prism structures. Six triangular prism structures are also tightly bonded together to form a complex metamaterial structure (Fig. 4D). After sequential stimulation of opposing magnetic field, continuous and abrupt structural changes happen together. The metamaterial structure shrinks apparently and exhibits dexterous structural changes. Even after many cycles of stimulation, the shape and deformation of the metamaterial structure remain stable, further demonstrating the excellent stickiness of the double-sided tape. Therefore, our proposed method can easily achieve uniform and nonuniform magnetization assembly for programmable soft robots with 2D and 3D geometries.

### Multiple module integration

We also achieve compatible integration of functional modules (temperature sensing modules, UV light sensing modules, pH sensing module, circuit module, positioning module, and oil sensing module) into regions of the multilegged soft robot that are not occupied by NdFeB microparticles (Fig. 5A). These regions have robust tackiness due to the presence of the adhesive tape. Considering the seamless integration and replaceability of all functional modules, temperature sensing and UV light sensing materials (power) are first incorporated into the one side of double-sided tape, and pH sensing module and oil sensing module (PDMS foam) are endowed with stickiness by depositing a layer of spray-on adhesive (fig. S14). In particular, circuit modules (copper conductive tape) and positioning modules (RFID) as commercial products have an adhesive sticker layer. Figure 5B exhibits the optical images of these functional modules. Thus, these functional modules can be seamlessly integrated onto soft robots by the close interaction of self-adhesive on functional modules and soft robots in a compatible way.

Next, we demonstrate the potential applications of the multifunctional multilegged soft (MFMLS) robot. The MFMLS robot is flexibly actuated using a cuboid magnet (length: 40 mm; width: 40 mm; height: 25 mm) and is capable of multimodal locomotion, which includes crawling, locomotion, and diving (fig. S15). For crawling on a dry surface (fig. S15A), the MFMLS robot will perceive the surrounding environment (Fig. 5, C and D). When the MFMLS robot approaches the heating area (65°C), the closest temperature sensing modules (35°C) will change their color from light blue to dark blue (blue arrows, Fig. 5C and movie S4). Next, the closest temperature sensing modules (65°C) change their color from light purple to deep purple when it first touches the heating area (purple arrows, Fig. 5C and movie S4). As the whole MFMLS robot enters the heating area, all temperature

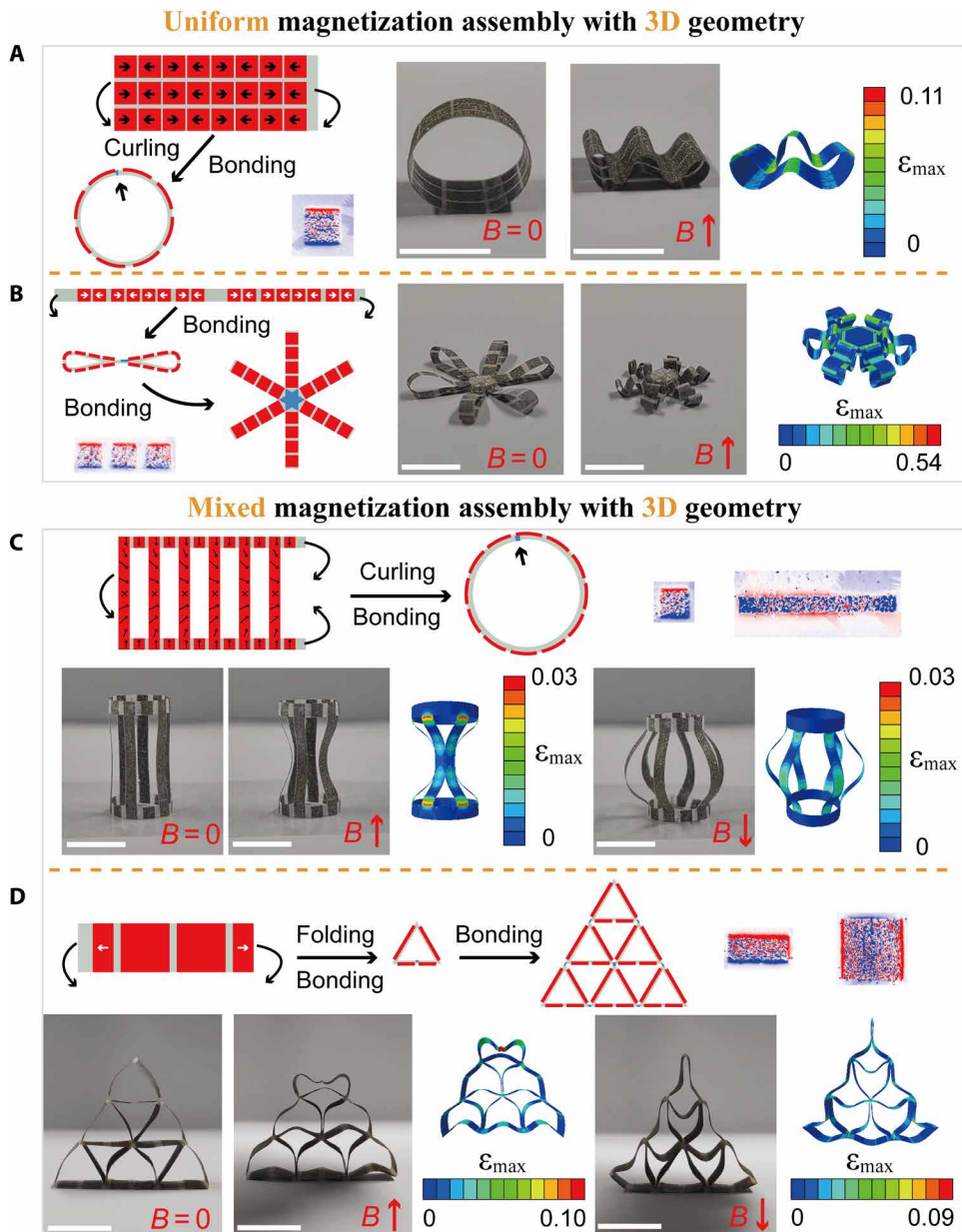


**Fig. 4. The soft robots with uniform and nonuniform magnetization assembly and 3D geometries.** The designed shapes with distributed magnetizations, bonding processes, optical images before and after magnetic stimulus and simulated deformation results of soft robots with 3D geometries fabricated by (**A** and **B**) discrete magnetization assembly and (**C** and **D**) mixed magnetization assembly. [Scale bars, 1 cm; color bars, the range of maximum principal strain (logarithmic strain)].

sensing modules change their colors. Thus, we acquire the ambient temperature information from the color feedback of robot to determine the following behaviors of MFMLS robot or judge whether it is safe or not. To improve the spatial resolution and precision of sensing, temperature sensing modules are uniformly distributed onto each leg to achieve multidirectional temperature sensing (Fig. 5, A and C). Similarly, UV light sensing modules are also uniformly distributed onto each leg to achieve multidirectional UV light sensing. When the MFMLS robot encounters UV light, the corresponding modules will quickly change their color from white to green (Fig. 5D and movie S4).

The MFMLS robot can also be used for water quality sensing through coupling with its multimodal motion. Because of its lightweight, large contact area with water, and the hydrophobicity of double-sided tape (fig. S16), the MFMLS robot can float and swiftly move around on water when actuated by a moving magnet [Fig. 5E (1), fig. S15B, and movie S6]. Once reaching the monitoring area, we judge the pH value ( $pH > 7$ ) of water according to the color change (from yellow to brown) of pH sensing modules. As the MFMLS robot deforms, the hydrophilic pH sensing modules adsorb the water to detect its pH value. The MFMLS robot also can dive into the water when actuated it from the bottom with a magnet [Fig. 5E(2) and

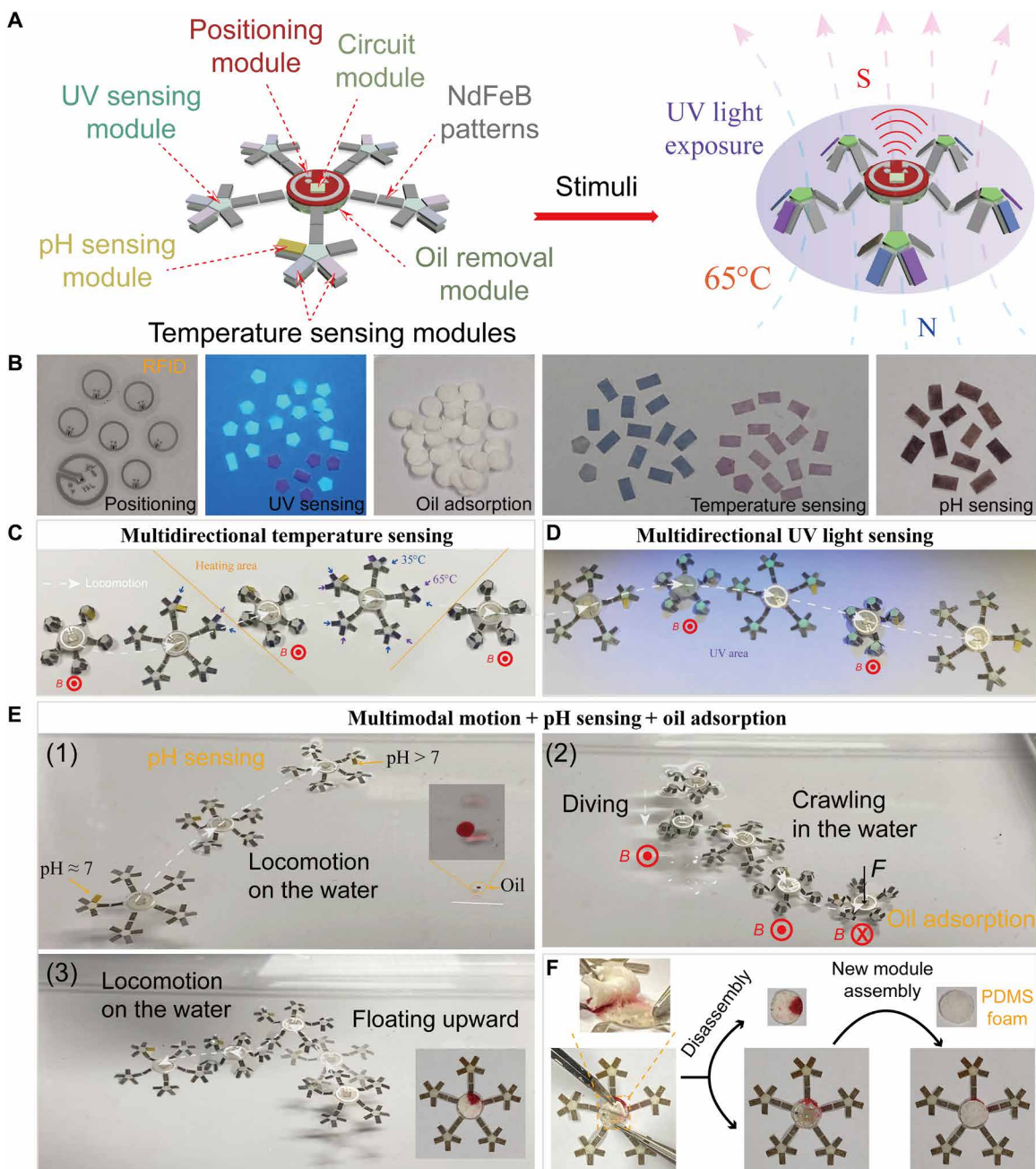


**Fig. 5. Multiple applications of MFMLS robot.** (A) The schematic diagram of MFMLS robot with functional modules (circuit, positioning, oil detection, temperature sensing, UV sensing, and pH sensing) and their response under various stimuli. N, North; S, South. (B) The optical images of all functional modules. (C) The multidirectional temperature sensing of MFMLS robot. (D) The multidirectional UV light sensing of MFMLS robot. (E) Multimodal motion for water quality testing of MFMLS robot: (1) the locomotion on the water and pH sensing, (2) the diving and crawling in the water and oil adsorption, and (3) the floating to the water surface (the inset image is the bottom view of MFMLS robot). (F) The replacement process of oil removal module (PDMS foam) after oil adsorption.

fig. S15C]. With the magnet approaching, the MFMLS robot shrinks its body to decrease the contact area with water. Meanwhile, the magnet provides a downward pulling force that overcomes the buoyancy of the MFMLS robot (its body and PDMS foam) to enable diving (movie S6). The PDMS foam is hydrophobic and lipophilic (fig. S15). Afterward reaching the bottom, the MFMLS robot reverts to a crawling gait and moves to the monitoring area. By applying opposing magnetic force, the oil sensing module is pressed to closely contact the

monitoring area to adsorb oil [Fig. 5E(2), fig. S14E, and movie S6]. After that, the MFMLS robot is controlled to float up from the bottom to the water surface without sinking [Fig. 5E (3) and fig. S15D]. The MFMLS robot is retrieved to observe whether there is oil exposure in the monitoring area [the inset image of Fig. 5E (3)]. After being used, the pH and oil sensing modules are easily peeled off and replaced by new ones for further use. Figure 5F displays the replacement process of the oil sensing module (PDMS foam). The PDMS

foam is wholly removed from the MFMLS robot, and no apparent residual is observed owing to the recyclability of adhesive sticker (the inset images in Fig. 5F). Thus, new PDMS foam can be tightly integrated into the MFMLS robot to conduct another test for measuring the presence of oil. The pH sensing module can also be replaced using the same process.

### Circuit repair in narrow and opaque space

The introduction of modular units for circuit functionality and repair represents another promising use case for soft magnetic robots (50, 51). Here, we use a commercial RFID tag to augment the capabilities of the MFMLS robot. The RFID tag is integrated at the center of MFMLS robot, and the circuit module is attached to its center. We assume that the failure point (open circuit) within an opaque channel can be observed by metal flaw detector. Thus, the RFID reader is positioned at the bottom of the channel in a manner that it faces the failure point in the channel. Under the joint action of the positioning module, circuit module, and MFMLS robot locomotion, we implement a temporary circuit connection at the failure point of the hard-to-reach region to deal with emergencies (Fig. 6A). Because of the small height of the MFMLS robot with magnetic actuation and its excellent locomotion capability, the MFMLS robot can easily enter the narrow channel and approach the failure point (Fig. 6, B and C, and fig. S17). During the approach process, we use the Received Signal Strength Indicator (RSSI) value obtained from the RFID reader to judge whether the circuit module is positioned below the failure point (Fig. 6B). The RSSI value first increases and then decreases to the lowest value ( $-42.0 \text{ dBm}$ ), which is used to determine the center of the robot (Fig. 6, D and E). If the RSSI value is larger than  $-42.0 \text{ dBm}$ , then the MFMLS robot is actuated to keep going forward. If the RSSI value is equal to  $-42.0 \text{ dBm}$ , then the position of MFMLS robot is slightly adjusted to observe whether the RSSI value changes gradually. If it changes, then the robot should keep moving forward. By repeating this process, if the RSSI value ( $-42.0 \text{ dBm}$ ) remains constant (red dotted frame of Fig. 6E), then we conclude that the center of the MFMLS robot is directly below the failure point. After a stronger magnetic actuation, the MFMLS robot is tightly pushed against the failure point to guarantee close contact between circuit modules and failure point, thereby restoring the circuit connection. This is evidenced by reactivation of the light-emitting diode (LED), which lights up again upon connecting (Fig. 6D and movie S5). Although previous works have demonstrated the ability to use soft robots to repair circuit connections, those implementations required manual position through visual inspection using the naked eye (48). Because those implementations require direct line of sight, the failure point cannot be observed in the case of an opaque channel or the presence of occlusions. Here, the RFID acts as an “eye” to help the user judge the position of the failure point. The MFMLS robot also can be controlled to come out from the narrow channel. As before, the RSSI value is observed to first increase and then decrease (Fig. 6E). Alternatively, the circuit module can also be replaced by liquid metal and conductive silver paste to achieve permanent circuit connecting. However, such materials might smear off the MFMLS robot and coat other contacting surfaces during locomotion.

### Therapy patch transfer in stomach

We further investigate the biomedical application of the modular magnetic soft robot. Because it is capable of multimodal locomotion, cargo delivery, and tolerating exposure to acid, the soft robot is well suited

for biomedical applications that involve operation in the stomach such as gastric ulcer treatment. More than 10% of people worldwide have suffered from gastric ulcers with high morbidity (52, 53). Drug therapy for effective acid suppressants is currently a common treatment method to decrease the incidence (53). However, long-term use of nonsteroidal anti-inflammatory drugs may result in life-threatening gastric bleeding (54). Coating technologies assisted with gastroscopy have been widely explored for ulcer treatment (55). Such an approach has the potential to stop bleeding, repel gastric fluids, promote tissue regeneration, and resist biofouling and inflammation. Nonetheless, conventional gastroscopy brings the risk of several complications and reduces the patient’s compliance (53). A wireless capsule endoscope has been developed to examine the gastrointestinal tract with painless procedure and higher safety, but other functions like endoscopic surgery for patch coating cannot be expanded (56). Thus, we propose to use a small untethered soft robot to replace the surgical stapler for coating a therapy patch onto gastric ulcer ex vivo. We anticipate that the combination of soft robot and capsule endoscope will become an ideal tool for painless treatment of gastrointestinal ulcers in the future. Compared to other soft robots (particularly gas-powered soft robots), our proposed soft robot is untethered and is wirelessly actuated by magnetic fields to achieve several actuation modes. These actuation modes not only can be used synergistically to overcome the complex terrain in the stomach to reach the target site but also can protect a therapy film and transfer it on the ulcer.

The soft robot is fabricated by incorporating magnetized NdFeB patterns (NdFeB size:  $150.0 \mu\text{m}$ ) into the two sides of double-sided tape (thickness:  $0.1 \text{ mm}$ ) (Fig. 7A). The larger NdFeB particles provide a stronger magnetic force to resist the adhesion of gastric mucosa to move flexibly. We measured the areal mass density of NdFeB microparticles (the mass of NdFeB microparticles adhered onto per square centimeter of tape) with different average sizes of  $38.0$ ,  $75.0$ , and  $150.0 \mu\text{m}$  to be  $6.837$ ,  $7.991$ , and  $9.791 \text{ mg cm}^{-2}$ , respectively. The areal mass density increases with increasing NdFeB particle sizes. At the same magnetizing condition, larger mass of NdFeB particles will produce stronger magnetic force (see more discussion in text S2). Meanwhile, the thicker double-sided tape also reduces the adhesion of gastric mucosa. The soluble tape is used as a sacrificial layer to temporarily fix the therapy patch. The therapy patch is a piece of cellulose film contained with drugs used for the treatment of gastric ulcers. Because of the thinner thickness of therapy patch, it can be tightly attached to the soluble tape. However, a soluble tape with low stickiness is easy to fall off during locomotion if it is directly taped onto the soft robot. Thus, these regions without NdFeB particles are reserved to tightly stick the soluble tape considering the excellent stickiness of adhesive sticker (the front side of the soft robot in Fig. 7A).

The soft robot mainly has five kinds of deformed structures (original, O-shaped, M-shaped, W-shaped, and semi-curled structures) (Fig. 7B). These deformations and the actuation of the soft robots are achieved by manually controlling a magnet. The O-shaped deformation is achieved by rotating a magnet through one circular revolution along its horizontal axis at the bottom of soft robot. The M-shaped deformation is achieved by placing a magnet with S-pole upward to approach the soft robot from the bottom. The W-shaped deformation is achieved by placing a magnet with its N-pole upward while approaching the soft robot from its bottom. The semi-curled deformation is achieved by rotating a magnet half a revolution along its horizontal axis at the bottom of the soft robot and then approaching the soft robot. By using these five structures, we have achieved six actuation modes of

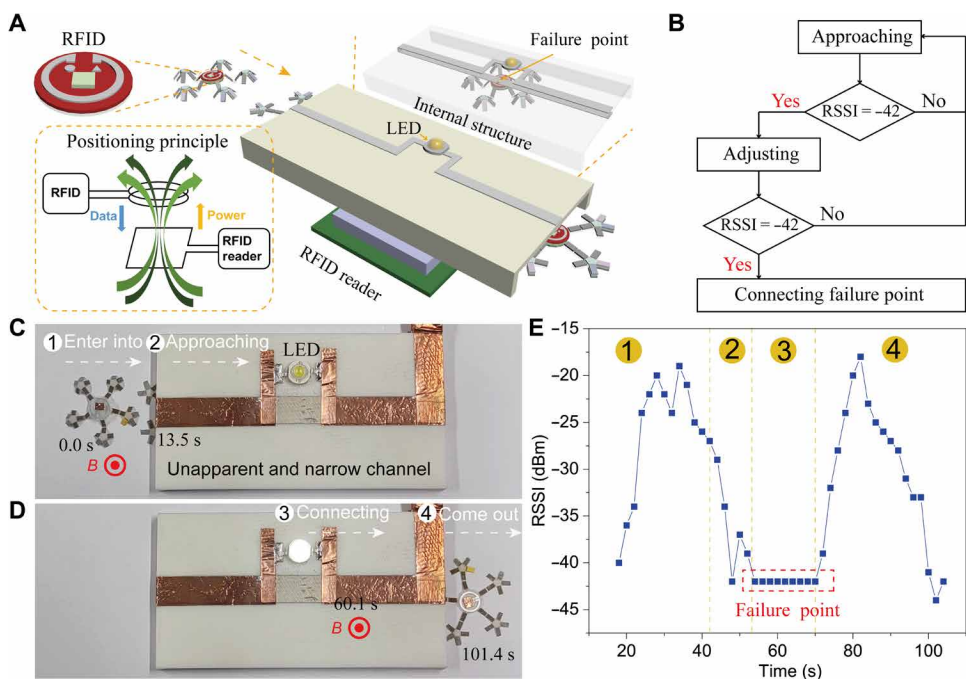


**Fig. 6. The circuit repairing process in a narrow and hard-to-reach space.** (A) The connecting of failure point in a hard-to-reach region by the joint action of robot's locomotion, circuit module, and positioning module (the inset images are the internal structure of the region and the positioning principle). (B) The logical process to judge the position of MFMLS robot by RSSI value. (C) The entering and approaching process of MFMLS robot to the failure point. (D) The process of failure point connecting and coming out. (E) The real-time RSSI value recorded by the RFID reader (the red dashed box indicates that the center of the robot is below the failure point).

the soft robots on a fresh pig stomach filled with mucosa, including curling, rolling, unfolding, climbing, turning over, and slipping (Fig. 7C, movie S7, and fig. S18). In the curling and rolling process, the therapy patch is wrapped in the middle of the soft robot to reduce the influence of gastric fluids. When the soft robot cannot pass the gastric fold by rolling, it will unfold itself and then climb through the fold by alternating W-shaped and M-shaped deformations. The therapy patch prefers to face upward after unfolding due to the residual stress in the O-shaped structures, which avoids direct contact between the therapy patch and mucosa and reduces the influence of gastric fluids. During the turning over process, the soft robot first transforms into the partially curved structure to ensure a high success rate. In addition, the structure of the soft robot is quickly adjusted to be a W-shaped structure after turning over, which is also maintained during slipping to keep the therapy patch away from the mucosa. As demonstrated in Fig. 7D, the multimodal locomotion enables the successful transfer and coating of the therapy patch on the gastric ulcer as well as the return of the soft robot after completing the task (Fig. 7D). Figure 7 (E and F) displays the transfer process and return process, respectively. All these processes are divided into six stages and achieved by the combination of different actuation modes. The detailed actuation steps of every stage can be found in fig. S19.

When the soft robot reaches the gastric ulcer in the transfer process, the soluble tape dissolves completely in the gastric mucosa to release the therapy patch. The inset image of Fig. 7F clearly shows that the gastric ulcer on the gastric fold is completely covered by the therapy patch. Considering that the capsule endoscope cannot be precisely controlled to track the locomotion of soft robot, we demonstrate the concept of the combination of the robot and the endoscope by using an ultrafine wired endoscope (diameter: 3.9 mm).

The pig stomach is expanded by blowing the air to form the real 3D structures (Fig. 7G). Under the vision of the endoscope, we have also realized the discovery of gastric ulcer and the tracking of the soft robot (Fig. 7H). The therapy patch is also successfully placed on the surface of the gastric ulcer. With innovations in capsule endoscopy for real-time visualization and tracking, we believe that there are further opportunities to improve the application of magnetic soft robots for minimally invasive treatments and therapy.

## DISCUSSION

Constructing magnetically driven intelligent soft robots with programmable shape morphing, multimodal locomotion, and multiple functions has the potential to enable advanced applications of soft robots in a wide variety of science and engineering fields. Programming discrete and continuous magnetization and introducing functional modules to soft robots are crucial. Although some efforts have been devoted to developing multifunctional soft robots, the open challenges of limited magnetization assembly, demanding operation, extra connecting steps, and easy delamination have restricted their further innovation.

We directly and seamlessly incorporate magnetized patterns composed of NdFeB microparticles into a network of adhesive sticker to fabricate soft robots with programmable magnetization profiles (uniform and nonuniform) with 2D or 3D geometries. These soft robots with different thicknesses exhibit dexterous structural changes. In addition, some regions without magnetic response are selectively reserved for introducing functional modules. We have integrated various functional modules with different material properties and forms (particles, papers, films, foams, circuit, and electronic components)

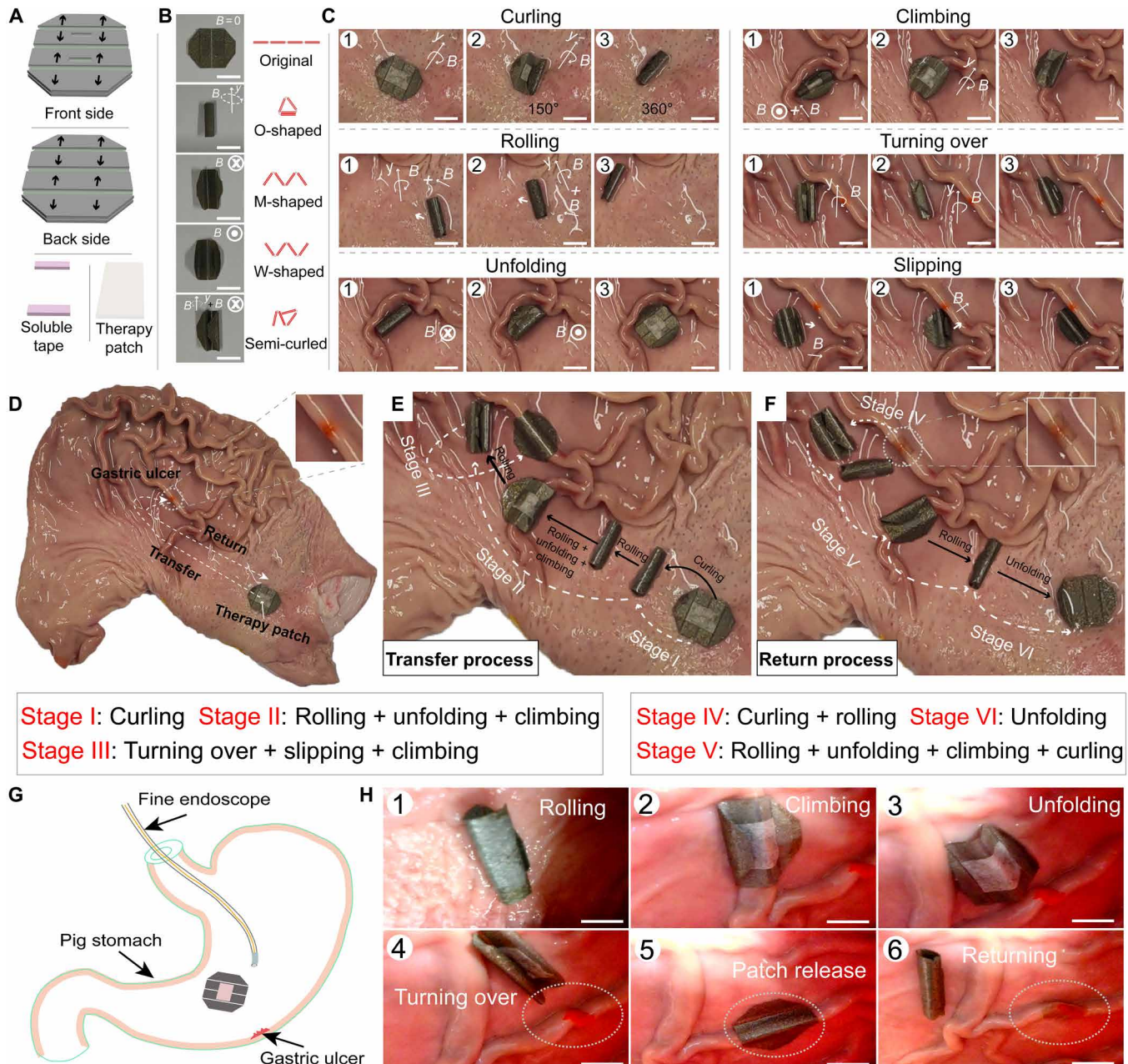


**Fig. 7. The therapy patch transfer by soft robot in stomach.** (A) The back and front sides of the soft robot. (B) Five mainly deformed structures of soft robot controlled by a magnet. (C) Six actuation modes of soft robot in stomach. (D) The total process for covering gastric ulcer by therapy patch with the soft robot. (E) The transfer process (stages I, II, and III) and (F) the return process (stages IV, V, and VI) of soft robot. (G) The schematic diagram of the combination of soft robot and endoscope. (H) Multimodal actuation under the observation by endoscope. (Scale bars, 1 cm)

into soft robots to explore their multimodal motions and applications in environmental sensing (temperature and UV light) and detection (pH and oil spilling), positioning, circuit repair, and gastric ulcer coating. All these assembly processes (NdFeB patterns and functional modules) are simple, requiring no extra connecting step. Meanwhile, all functional modules do not spontaneously delaminate unless they are forcefully peeled off for replacement. The proposed strategy simplifies the fabrication of multifunctional soft robots and provides more freedom in prescribing magnetization profiles and

expands the range of possibilities for function integration. We believe that it will inspire and enable more intelligent soft robots with specialized functions, improved environmental adaptability, and fast iterative feedback.

In this work, we exhibit the concept of functional integration by using some basic modules. For realizing further intelligence of soft robots, a broad range of electronic components and wireless systems with high performance may afford many possibilities in functional integration (50, 51, 57). Potential electronic components include

silicon infrared LED, complementary metal-oxide semiconductor transistors, UV sensors, temperature sensors, and microsupercapacitors; these wireless systems include energy receiver coils, inductor coils, near-field communication, RFID, and so on. We anticipate that several electronic components and wireless systems can be rationally designed and assembled onto the magnetically actuated soft robots to work synergistically for multifunctional applications, autonomous behaviors, or specific tasks. A fully autonomous system-engineered miniaturized robot may be developed in the future (58). Some modules that cannot be given stickiness have difficulty integrating onto the soft robots. For example, hydrogel-based materials, as important materials for biomedical applications, are hard to be directly integrated onto the soft robots. Meanwhile, the overall architecture of the functional soft robots fabricated using our proposed approach is modular but can be challenging to downscale when smaller soft robots are needed for biomedical applications in lumens of human body, such as urogenital system, gastrointestinal tract, auditory meatus, nasal cavity, etc. Since the fabrication accuracy of NdFeB patterns is about 50  $\mu\text{m}$ , the size of the assembled soft robots will not be less than 100  $\mu\text{m}$  when only two patterns are assembled. The introduction of on-chip fabrication technology and rolled-up technology may be a good choice to solve the problem (57). The downscaled size of soft robots also brings new challenges of precise modular integration and cutting contour of soft robots. Current or new technologies need to be explored to overcome these challenges.

In addition, when several identical robots are in the same magnetic field, it is not possible to individually operate more than one robot at a time. However, soft robots with different magnetization profiles and geometries may exhibit different deformations and locomotion behaviors in response to the same magnetic field. Rational design in magnetization profiles and geometries is needed for soft robots to perform their functions individually. The programmability of magnetization profiles within soft robots may provide them with more possibilities in terms of their deformation modes and corresponding applications. However, the magnetization profiles of soft robots fabricated using our proposed approach are fixed, which have limited their functions. This could potentially be solved by locally changing the physical properties of adhesive stickers and further rearranging the magnetization profiles.

## MATERIALS AND METHODS

### The fabrication of NdFeB patterns

First, wax pattern that is complementary to the NdFeB patterns is printed onto the PEI tape. The wax pattern can be recognized as a mask. Next, NdFeB microparticles with different average sizes of 38.0, 75.0, and 150.0  $\mu\text{m}$  are added onto the PEI tape. After pressing, a part of NdFeB microparticles stick onto the region of PEI tape without wax, and the free NdFeB microparticles are easy to remove. Then, the PEI tape with NdFeB microparticles is soaked into the ethyl acetate solution for 5 min. After slightly shaking, the wax pattern will drop off from the PEI tape, and the NdFeB patterns will form on the PEI tape.

### The fabrication of magnetized NdFeB patterns

According to the deformation requirement of soft robots actuated by magnetic fields, the 2D planar shapes and 3D structures of soft robots are first divided into individual NdFeB patterns. Next, these NdFeB patterns are fabricated and magnetized by a magnetizer

(MA 2030, Shenzhen Jiuju Industrial Equipment Co. Ltd.) to acquire the programmable magnetization. For the uniform magnetization (in-plane and out-of-plane magnetization), the NdFeB/PEI film with the same NdFeB patterns is directly adhered onto a glass slide or template along its long edge (relying on the stickiness of the PEI tape) and then fixed onto the magnetizer. By adjusting the height and intersection angle between NdFeB patterns and inductor coil, the uniform magnetization is acquired after magnetizing. The height and intersection angle determine the strength and direction of the magnetic field within NdFeB patterns. For nonuniform magnetization, the NdFeB/PEI film with the same or single NdFeB patterns is adhered onto the 3D-printed template along its curved structure to complete the magnetization.

### The fabrication of programmable magnetic soft robots

The programmable magnetic soft robots can be fabricated with mass production and high reproducibility by using roll-to-roll technology. The magnetized NdFeB patterns with different magnetization profiles are first fixed onto the PEI tape and then wrapped onto different rollers according to the shape and the position of individual magnetization profiles of soft robots. After that, one of the fabricated rollers is installed onto the homemade roll-to-roll device to achieve the transfer of magnetized NdFeB patterns into the specific position of the double-sided tape. By repeating the process, magnetized NdFeB patterns can be assembled one by one into the same double-sided tape to form the corresponding programmable soft robots.

The programmable magnetic soft robots can also be fabricated manually. The planar shapes of these soft robots are first designed by drawing software and then printed onto an A4 paper. Next, a piece of double-sided tape is taped onto the printed planar shapes. After that, magnetized NdFeB patterns with different magnetization profiles are assembled onto the double-sided tape one by one. The printed planar shapes are used to ensure assembly accuracy. In this process, NdFeB patterns should be tightly pressed and scratched to ensure successful transfer of NdFeB microparticles into the network of double-sided tape. Last, the assembled magnetic soft robots are acquired by cutting along the outline of planar shapes and then peeling off from the A4 paper.

### Simulations of deformations

The deformation of the magnetic soft robot under static magnetic field was conducted using a UEL in ABAQUS. The simulations include the following parameters: the shear modulus  $\mu$ , the strength of external magnetic field  $B$ , and the remanence  $M$  of the material. We divide the whole structure into magnetic regions and nonmagnetic regions according to the distribution of the magnetic modules. The shear moduli for the magnetic and nonmagnetic sections are 156 and 126 kPa, respectively. We characterized the modulus using a Tinius Olsen H5KS material testing system. The materials in the simulation are assumed to be incompressible and fit the neo-Hookean material model. The remanences of the magnetic region and nonmagnetic region are set to be 73.7 and 0 kA/m, respectively. Considering the possible asymmetry of Cauchy stress induced by magnetic body torques, customized eight-noded brick elements are used to handle the nine components of the Cauchy stress tensor.

### The fabrication of functional modules

The temperature sensing modules and UV light sensing modules are fabricated by incorporating commercially available temperature

sensing power and UV light sensing powder into the self-adhesive network of double-sided tape with the thickness of 30  $\mu\text{m}$  and then cutting into the many rectangular or pentagonal shapes. The power is easily incorporated into the network and onto the surface of double-sided tape. The pH sensing modules are fabricated by spraying a layer of self-adhesive onto the pH testing paper and then cutting it into a lot of small rectangular shapes.

The oil sensing modules (PDMS foam) are fabricated by emulsion method. Ten grams of PDMS prepolymer is first thoroughly mixed with a curing agent with a weight ratio of 10:1. Next, 12 g of paraffin oil is added into the mixture under vigorous stirring. Then, 75 g of distilled water is added dropwise under continuous stirring for 30 min to form PDMS-water emulsion. The emulsion is then poured into spaced glass pieces and heated at 70°C for 2 hours to conduct polymerization. The polymerized PDMS foam is released from the spaced glass pieces and then washed by ethanol to remove paraffin oil. The clean PDMS foam is acquired after heating at 70°C for 6 hours to remove remaining ethanol. Last, the PDMS foam is cut into small round pieces and sprayed a layer of self-adhesive.

## SUPPLEMENTARY MATERIALS

Supplementary material for this article is available at <https://science.org/doi/10.1126/sciadv.abn8932>

## REFERENCES AND NOTES

- W. Hu, G. Z. Lum, M. Mastrangeli, M. Sitti, Small-scale soft-bodied robot with multimodal locomotion. *Nature* **554**, 81–85 (2018).
- T. Xu, J. Zhang, M. Salehzadeh, O. Onaizah, E. Diller, Millimeter-scale flexible robots with programmable three-dimensional magnetization and motions. *Sci. Robot.* **4**, eaav4494 (2019).
- Y. Alapan, A. C. Karacakol, S. N. Guzelhan, I. Isik, M. Sitti, Reprogrammable shape morphing of magnetic soft machines. *Sci. Adv.* **6**, eabc6414 (2020).
- Y. Dong, J. Wang, X. Guo, S. Yang, M. O. Ozen, P. Chen, X. Liu, W. Du, F. Xiao, U. Demirci, B.-F. Liu, Multi-stimuli-responsive programmable biomimetic actuator. *Nat. Commun.* **10**, 4087 (2019).
- C. Li, G. C. Lau, H. Yuan, A. Aggarwal, V. L. Dominguez, S. Liu, H. Sai, L. C. Palmer, N. A. Sather, T. J. Pearson, D. E. Freedman, P. K. Amiri, M. O. De La Cruz, S. I. Stupp, Fast and programmable locomotion of hydrogel-metal hybrids under light and magnetic fields. *Sci. Robot.* **5**, eaabb9822 (2020).
- Y. Dong, L. Wang, N. Xia, Y. Wang, S. Wang, Z. Yang, D. Jin, X. Du, E. Yu, C. Pan, B.-F. Liu, L. Zhang, Multi-stimuli-response programmable soft actuators with site-specific and anisotropic deformation behavior. *Nano Energy* **88**, 106254 (2021).
- F. Ji, T. Li, S. Yu, Z. Wu, L. Zhang, Propulsion gait analysis and fluidic trapping of swinging flexible nanomotors. *ACS Nano* **15**, 5118–5128 (2021).
- Y. Kim, H. Yuk, R. Zhao, S. A. Chester, X. Zhao, Printing ferromagnetic domains for untethered fast-transforming soft materials. *Nature* **558**, 274–279 (2018).
- H. Deng, K. Sattari, Y. Xie, P. Liao, Z. Yan, J. Lin, Laser reprogramming magnetic anisotropy in soft composites for reconfigurable 3D shaping. *Nat. Commun.* **11**, 6325 (2020).
- Q. Ze, X. Kuang, S. Wu, J. Wong, S. M. Montgomery, R. Zhang, J. M. Kovitz, F. Yang, H. J. Qi, R. Zhao, Magnetic shape memory polymers with integrated multifunctional shape manipulation. *Adv. Mater.* **32**, 1906657 (2020).
- Y. Zhao, S. Gao, X. Zhang, W. Huo, H. Xu, C. Chen, J. Li, K. Xu, X. Huang, Fully flexible electromagnetic vibration sensors with annular field confinement origami magnetic membranes. *Adv. Funct. Mater.* **30**, 2001553 (2020).
- D. Jin, J. Yu, K. Yuan, L. Zhang, Mimicking the structure and function of ant bridges in a reconfigurable microswarm for electronic applications. *ACS Nano* **13**, 5999–6007 (2019).
- X. Yang, W. Shang, H. Lu, Y. Liu, L. Yang, R. Tan, X. Wu, Y. Shen, An agglutinate magnetic spray transforms inanimate objects into millirobots for biomedical applications. *Sci. Robot.* **5**, eabc8191 (2020).
- J. Zhang, Z. Ren, W. Hu, R. H. Soon, I. C. Yasa, Z. Liu, M. Sitti, Voxelated three-dimensional miniature magnetic soft machines via multimaterial heterogeneous assembly. *Sci. Robot.* **6**, eabf0112 (2021).
- Z. Zheng, H. Wang, L. Dong, Q. Shi, J. Li, T. Sun, Q. Huang, T. Fukuda, Ionic shape-morphing microrobotic end-effectors for environmentally adaptive targeting, releasing, and sampling. *Nat. Commun.* **12**, 411 (2021).
- A. Ghosh, L. Li, L. Xu, R. P. Dash, N. Gupta, J. Lam, Q. Jin, V. Akshintala, G. Pahapale, W. Liu, A. Sarkar, R. Rais, D. H. Gracias, F. M. Selaru, Gastrointestinal-resident, shape-changing microdevices extend drug release in vivo. *Sci. Adv.* **6**, eabb4133 (2020).
- B. Wang, K. Kostarelos, B. J. Nelson, L. Zhang, Trends in micro-/nanorobotics: Materials development, actuation, localization, and system integration for biomedical applications. *Adv. Mater.* **33**, 2002047 (2021).
- A. S. Gladman, E. A. Matsumoto, R. G. Nuzzo, L. Mahadevan, J. A. Lewis, Biomimetic 4D printing. *Nat. Mater.* **15**, 413–418 (2016).
- B. Han, Y. L. Zhang, L. Zhu, Y. Li, Z. C. Ma, Y. Q. Liu, X. L. Zhang, X. W. Cao, Q. D. Chen, C. W. Qiu, H. B. Sun, Plasmonic-assisted graphene oxide artificial muscles. *Adv. Mater.* **31**, 1806386 (2019).
- J. Cui, T.-Y. Huang, Z. Luo, P. Testa, H. Gu, X.-Z. Chen, B. J. Nelson, L. J. Heyderman, Nanomagnetic encoding of shape-morphing micromachines. *Nature* **575**, 164–168 (2019).
- H.-W. Huang, M. S. Sakar, A. J. Petruska, S. Pané, B. J. Nelson, Soft micromachines with programmable motility and morphology. *Nat. Commun.* **7**, 12263 (2016).
- Z. Li, Z. Ye, L. Han, Q. Fan, C. Wu, D. Ding, H. L. Xin, N. V. Myung, Y. Yin, Polarization-modulated multidirectional photothermal actuators. *Adv. Mater.* **33**, 2006367 (2021).
- B. Wang, K. F. Chan, K. Yuan, Q. Wang, X. Xia, L. Yang, H. Ko, Y.-X. J. Wang, J. J. Y. Sung, P. W. Y. Chiu, L. Zhang, Endoscopy-assisted magnetic navigation of biohybrid soft microrobots with rapid endoluminal delivery and imaging. *Sci. Robot.* **6**, eabd2813 (2021).
- M. Li, A. Pal, A. Aghakhani, A. Pena-Francesch, M. Sitti, Soft actuators for real-world applications. *Nat. Rev. Mater.* **7**, 235–249 (2022).
- G.-Z. Yang, J. Bellinger, P. E. Dupont, P. Fischer, L. Floridi, R. Full, N. Jacobstein, V. Kumar, M. McNutt, R. Merrifield, B. J. Nelson, B. Scasselati, M. Taddeo, R. Taylor, M. Veloso, Z. L. Wang, R. Wood, The grand challenges of Science Robotics. *Sci. Robot.* **3**, eaar7650 (2018).
- E. W. Hawkes, C. Majidi, M. T. Tolley, Hard questions for soft robot. *Sci. Robot.* **6**, eabg6049 (2021).
- S. Zhang, X. Ke, Q. Jiang, H. Ding, Z. Wu, Programmable and reprocessable multifunctional elastomeric sheets for soft origami robots. *Sci. Robot.* **6**, eabd6107 (2021).
- S. Sundaram, M. Skouras, D. S. Kim, L. van den Heuvel, W. Matusik, Topology optimization and 3D printing of multimaterial magnetic actuators and displays. *Sci. Adv.* **5**, eaaw1160 (2019).
- M. A. Skylar-Scott, J. Mueller, C. W. Visser, J. A. Lewis, Voxelated soft matter via multimaterial multinozzle 3D printing. *Nature* **575**, 330–335 (2019).
- H. Lee, Y. Jang, J. K. Choe, S. Lee, H. Song, J. P. Lee, N. Lone, J. Kim, 3D-printed programmable tensegrity for soft robotics. *Sci. Robot.* **5**, eaay9024 (2020).
- D. Jin, K. Yuan, X. Du, Q. Wang, S. Wang, L. Zhang, Domino reaction encoded heterogeneous colloidal microswarm with on-demand morphological adaptability. *Adv. Mater.* **33**, 2100070 (2021).
- C. Majidi, Soft robotics: A perspective—Current trends and prospects for the future. *Soft Robot.* **1**, 5–11 (2014).
- P. Rothemund, Y. Kim, R. H. Heisser, X. Zhao, R. F. Shepherd, C. Keplinger, Shaping the future of robotics through materials innovation. *Nat. Mater.* **20**, 1582–1587 (2021).
- Y. Zhang, Q. Wang, S. Yi, Z. Lin, C. Wang, Z. Chen, L. Jiang, 4D printing of magnetoactive soft materials for on-demand magnetic actuation transformation. *ACS Appl. Mater. Inter.* **13**, 4174–4184 (2021).
- C. Ma, S. Wu, Q. Ze, X. Kuang, R. Zhang, H. J. Qi, R. Zhao, Magnetic multimaterial printing for multimodal shape transformation with tunable properties and shiftable mechanical behaviors. *ACS Appl. Mater. Inter.* **13**, 12639–12648 (2020).
- X. Kuang, S. Wu, Q. Ze, L. Yue, Y. Jin, S. M. Montgomery, F. Yang, H. J. Qi, R. Zhao, Magnetic dynamic polymers for modular assembling and reconfigurable morphing architectures. *Adv. Mater.* **31**, 2102113 (2021).
- Y. Cheng, K. H. Chan, X. Q. Wang, T. Ding, T. Li, C. Zhang, W. Lu, Y. Zhou, G. W. Ho, A fast autonomous healing magnetic elastomer for instantly recoverable, modularly programmable, and thermorecyclable soft robots. *Adv. Funct. Mater.* **31**, 2101825 (2021).
- S. M. Montgomery, S. Wu, X. Kuang, C. D. Armstrong, C. Zemelka, Q. Ze, R. Zhang, R. Zhao, H. J. Qi, Magneto-mechanical metamaterials with widely tunable mechanical properties and acoustic bandgaps. *Adv. Funct. Mater.* **31**, 2005319 (2021).
- G. Z. Lum, Z. Ye, X. Dong, H. Marvi, O. Erin, W. Hu, M. Sitti, Shape-programmable magnetic soft matter. *Proc. Natl. Acad. Sci. U.S.A.* **113**, E6007–E6015 (2016).
- M. Wehner, R. L. Truby, D. J. Fitzgerald, B. Mosadegh, G. M. Whitesides, J. A. Lewis, R. J. Wood, An integrated design and fabrication strategy for entirely soft, autonomous robots. *Nature* **536**, 451–455 (2016).
- C. Wang, K. Sim, J. Chen, H. Kim, Z. Rao, Y. Li, W. Chen, J. Song, R. Verduzco, C. Yu, Soft ultrathin electronics innervated adaptive fully soft robots. *Adv. Mater.* **30**, 1706695 (2018).
- K. B. Justus, T. Hellebrekers, D. D. Lewis, A. Wood, C. Ingham, C. Majidi, P. R. LeDuc, C. Tan, A biosensing soft robot: Autonomous parsing of chemical signals through integrated organic and inorganic interfaces. *Sci. Robot.* **4**, eaax0765 (2019).

43. F. Fu, L. Shang, Z. Chen, Y. Yu, Y. Zhao, Bioinspired living structural color hydrogels. *Sci. Robot.* **3**, eaar8580 (2018).
44. Y. Kim, G. A. Parada, S. Liu, X. Zhao, Ferromagnetic soft continuum robots. *Sci. Robot.* **4**, eaax7329 (2019).
45. Y. Kim, E. Genevriere, P. Harker, J. Choe, M. Balicki, R. W. Regenhardt, J. E. Vranic, A. A. Dmytriw, A. B. Patel, X. Zhao, Telerobotic neurovascular interventions with magnetic manipulation. *Sci. Robot.* **7**, eabg9907 (2022).
46. R. Zhao, Y. Kim, S. A. Chester, P. Sharma, X. Zhao, Mechanics of hard-magnetic soft materials. *J. Mech. Phys. Solids* **124**, 244–263 (2019).
47. Y. Kim, X. Zhao, Magnetic soft materials and robots. *Chem. Rev.* **122**, 5317–5364 (2022).
48. X. Ke, S. Zhang, Z. Chai, J. Jiang, Y. Xu, B. Tao, H. Ding, Z. Wu, Flexible discretely-magnetized configurable soft robots via laser-tuned selective transfer printing of anisotropic ferromagnetic cells. *Mater. Today Phys.* **17**, 100313 (2021).
49. Y. Hu, Z. Wang, D. Jin, C. Zhang, R. Sun, Z. Li, K. Hu, J. Ni, Z. Cai, D. Pan, X. Wang, W. Zhu, J. Li, D. Wu, L. Zhang, J. Chu, Botanical-inspired 4D printing of hydrogel at the microscale. *Adv. Funct. Mater.* **30**, 1907377 (2020).
50. B. H. Kim, K. Li, J.-T. Kim, Y. Park, H. Jang, X. Wang, Z. Xie, S. M. Won, H.-J. Yoon, G. Lee, W. J. Jang, K. H. Lee, T. S. Chung, Y. H. Jung, S. Y. Heo, Y. Lee, J. Kim, T. Cai, Y. Kim, P. Prasopsukh, Y. Yu, X. Yu, R. Avila, H. Luan, H. Song, F. Zhu, Y. Zhao, L. Chen, S. H. Han, J. Kim, S. J. Oh, H. Lee, C. H. Lee, Y. Huang, L. P. Chamorro, Y. Zhang, J. A. Rogers, Three-dimensional electronic microfliers inspired by wind-dispersed seeds. *Nature* **597**, 503–510 (2021).
51. M. Z. Miskin, A. J. Cortese, K. Dorsey, E. P. Esposito, M. F. Reynolds, Q. Liu, M. Cao, D. A. Muller, P. L. McEuen, I. Cohen, Electronically integrated, mass-manufactured, microscopic robots. *Nature* **584**, 557–561 (2020).
52. J. H. Maeng, B. W. Bang, E. Lee, J. Kim, H. G. Kim, D. H. Lee, S.-G. Yang, Endoscopic application of EGF-chitosan hydrogel for precipitated healing of GI peptic ulcers and mucosectomy-induced ulcers. *J. Mater. Sci. Mater. Med.* **25**, 573–582 (2014).
53. Z. Cheng, R. Qing, S. Hao, Y. Ding, H. Yin, G. Zha, X. Chen, J. Ji, B. Wang, Fabrication of ulcer-adhesive oral keratin hydrogel for gastric ulcer healing in a rat. *Regen. Biomater.* **8**, rbab008 (2021).
54. J. H. Maeng, J. W. So, J. Kim, I. A. Kim, J. H. Jung, K. Min, D. H. Lee, S.-G. Yang, rhEGF-containing thermosensitive and mucoadhesive polymeric sol-gel for endoscopic treatment of gastric ulcer and bleeding. *J. Biomater. Appl.* **28**, 1113–1121 (2014).
55. S. J. Wu, H. Yuk, J. Wu, C. S. Nabzdyk, X. Zhao, A multifunctional origami patch for minimally invasive tissue sealing. *Adv. Mater.* **33**, 2007667 (2021).
56. J. Min, Y. Yang, Z. Wu, W. Gao, Robotics in the gut. *Adv. Ther.* **3**, 1900125 (2020).
57. V. K. Bandari, Y. Nan, D. Karnaushenko, Y. Hong, B. Sun, F. Striggow, D. D. Karnaushenko, C. Becker, M. Faghili, M. Medina-Sánchez, F. Zhu, O. G. Schmidt, A flexible microsystem capable of controlled motion and actuation by wireless power transfer. *Nat. Electron.* **3**, 172–180 (2020).
58. V. K. Bandari, O. G. Schmidt, System-engineered miniaturized robots: From structure to intelligence. *Adv. Intell. Syst.* **3**, 2000284 (2021).

#### Acknowledgments

**Funding:** This work was supported by the Hong Kong Research Grants Council (RGC) with project nos. JLFS/E-402/18, C1134-20GF, and E-CUHK401/20; the ITF project with project no. MRP/036/18X funded by the HKSAR Innovation and Technology Commission (ITC), the Croucher Foundation Grant with ref. no. CAS20403, and the CUHK internal grants. We also thank the support from the SIAT-CUHK Joint Laboratory of Robotics and Intelligent Systems and the Multi-scale Medical Robotics Centre (MRC), InnoHK, at the Hong Kong Science Park.

**Author contributions:** Y.D. conceived the idea and designed the experiments. Y.D., L.W., Z.Y., C.Z., and D.J. performed the experiments. Y.D., N.X., and Z.Y. conducted the simulated analysis. Y.D., L.W., C.P., J.Z., C.M., and L.Z. analyzed the experimental data and wrote the paper. L.Z. supervised the research. **Competing interests:** The authors declare that they have no competing interests. **Data and materials availability:** All data needed to evaluate the conclusions in the paper are present in the paper and/or the Supplementary Materials.

Submitted 28 December 2021

Accepted 6 May 2022

Published 22 June 2022

10.1126/sciadv.abn8932